Automatic segmentation of histological structures in normal and neoplastic mammary gland tissue sections

Rodrigo Fernandez-Gonzalez *[a, c], Thomas Deschamps[b], Adam Idica[a],
Ravi Malladi[b], Carlos Ortiz de Solorzano[a]

[a]Life Sciences Division, Lawrence Berkeley National Laboratory, Berkeley, CA 94720
[b]Mathematics Department, Lawrence Berkeley National Laboratory, Berkeley, CA 94720
[c]UC Berkeley /UC San Francisco Joint Graduate Group in Bioengineering, Berkeley, CA 94720

ABSTRACT

In this paper we present a scheme for real time segmentation of histological structures in microscopic images of normal and neoplastic mammary gland sections. Paraffin embedded or frozen tissue blocks are sliced, and sections are stained with hematoxylin and eosin (H&E). The sections are then imaged using conventional bright field microscopy. The background of the images is corrected by arithmetic manipulation using a "phantom". Then we use the fast marching method with a speed function that depends on the brightness gradient of the image to obtain a preliminary approximation to the boundaries of the structures of interest within a region of interest (ROI) of the entire section manually selected by the user. We use the result of the fast marching method as the initial condition for the level set motion equation. We run this last method for a few steps and obtain the final result of the segmentation. These results can be connected from section to section to build a three-dimensional reconstruction of the entire tissue block that we are studying.

Keywords: 3D reconstruction, background correction, brightness gradient, fast marching method, level set method

1. INTRODUCTION

The mature mammary gland has been characterized as a tree-like structure formed by hollow ducts converging at the nipple. From there a primary duct branches into secondary ones, which themselves form tertiary ducts. The ducts, lined by one or two layers of epithelial cells, finish in secretory structures known as terminal ductal lobular units, which are the site of milk production after pregnancy.

In cancer, this hierarchical structure is disrupted by an uncontrolled growth of the ductal epithelium from the lobular units into the ducts and the subsequent invasion of the surrounding tissue. Thus, morphological or structural changes accompany the genetic changes that occur in breast cancer.

An interesting problem is posed by the idea of quantifying these genetic or molecular changes that occur during breast cancer progression in the context of the tissue environment where they occur. This would allow studying the correlation between morphological and molecular mutations in breast cancer. Since the mammary gland and its constituent elements are neither flat nor homogenous, the approach to this problem should be three-dimensional, and take into account the heterogeneity of the gland. However, most biological methods focus on just one type of changes (molecular or morphological) and neglect three-dimensionality and heterogeneity.

Although imaging tissue structure and function *in vivo* would be extremely desirable, the existing *in vivo* imaging methods (X-ray, MRI, optical tomography, etc) don't provide the necessary resolution or penetration into the tissue for cell-level molecular analysis and/or require an imaging-forming substrate that can not be introduced in the tissue without severely altering its normal functioning. Consequently, *ex-vivo* microscopic analysis of the tissue from flat fixed sections is the routine method in histopathology. However, our limited ability for extrapolating and visualizing three-dimensional

---

* rfgonzalez@lbl.gov

information from sequences of two-dimensional scenes renders this method non suitable for quantitative three-dimensional tissue characterization.

To overcome these issues we have developed a system for simultaneous morphological and molecular analyses of thick tissue samples[1]. The system is composed of a computer-assisted microscope and a JAVA -based image display, analysis and visualization program that allows semi-automatic acquisition, annotation, storage, three-dimensional reconstruction and analysis of histological structures of interest (intraductal tumors, normal ducts, blood vessels, etc.) in thick tissue specimens. For this the tissue needs to be extracted from the donor and embedded in a permanent or semi-rigid medium before being fully sectioned. Then the sections have to be stained in a way that visually highlights the desired structures.

In this paper we will focus on the annotation of the structures of interest on the H&E stained sections. Manual segmentation has been used before to delineate histological structures[2,3] and therefore we initially annotated each of the interesting features of the tissue manually on each section in order to build the three-dimensional reconstruction of the block. This constituted the bottleneck in the study of samples. Semiautomatic approaches to segmentation of features of interest in histological sections have also been used[4], but they still involve a lot of user interaction, which remains the bottleneck in the process of analyzing samples. Automatic annotation (segmentation) of the structures of interest is the answer to this problem. Here we propose an automatic method followed by interactive correction that greatly reduces the interaction required, thus eliminating the bottleneck and opening the door to the use of our system for imaging and reconstruct large, complex tissue structures.

Active contour models[5] have been used before to segment objects from image data. These methods are based on deforming an initial "seed" curve towards the boundary of the desired object. The deformation is achieved by minimizing a certain energy function that approaches a minimum near the object boundary. However, these models only produce satisfactory results for smooth objects, failing to correctly delineate objects with big protrusions. Due to the existence of multiple local energy minima for this kind of objects, the result of the segmentation largely depends on how good the initial condition is, i.e., how close is the initial seed curve to the desired contour. Moreover, active contours are topologically constrained and cannot deal with multiple objects in a single image[6], thus requiring running an independent minimization process for each object/seed pair.

Given the limitations of all the above-mentioned methods, we proposed to use the level set approach[7,8] which is an interface propagation technique used for different applications, including segmentation. The initial curve is represented here as the zero level set of a higher dimensional function, and the motion of the curve is embedded within the motion of the higher dimensional surface. The speed of that motion is defined based on the characteristics of the image to be segmented, and thus adjusted so that when the interface passes over low brightness gradient areas the interface expands quickly, whereas when the gradient is large (indicating the location of an edge in the image) the curve is slowed down. In addition, a surface tension term (in the form of curvature) is included in the speed function to slightly retard the expanding contours at very high-gradient areas, which usually correspond to image noise. The interface can propagate within narrow regions, and is able to handle topological changes, thus being able to segment multiple objects simultaneously. In addition, handling an inherently two-dimensional problem in three dimensions by embedding the seed into a continuous surface facilitates calculating the curvature of the front and dealing with singularities in the evolution of the curve.

However, changing an n-dimensional problem into one in n+1 dimensions increases the computational cost. The narrow-band method accelerates the level set flow by updating the position of the curve only in a narrow vicinity of its current location. But in our experience, the narrow band technique does not reduce the computational cost to a reasonable limit, due to the large size of the images of the sections. Thus, we propose to use the fast marching method[9,10], a numerical technique to solve the equation that drives the movement of the curve by combining an efficient –constrained- solution to the equation of the movement of the front, narrow-band level set methods and a *min*-heap data structure. This method is only used for monotonically advancing fronts, providing a very fast solution, even though not as accurate as the one obtained by using the level set method. This solution is then used as the initial condition for the slower but more accurate full level set segmentation.

The rest of this paper is organized as follows: Section 2 describes the general tissue handling and image acquisition that we use, and the theoretical basis of the segmentation scheme. Section 3 shows the results of applying our method to histological tissue sections. Section 4 discusses the results and suggests some future developments and improvements to our technique.

2. METHODOLOGY

2.1 Tissue processing and imaging

The tissue processing and staining protocol that we use for the analysis is illustrated in figure 1. Tissue blocks of 4 to 5 mm of thickness are sliced into 5 μm (thin) sections. The odd sections are stained with H&E, which is the standard staining in routine histopathology. It provides morphological information both at the cytological (single cell) and architectural (organ) level. The even sections are stained using some fluorescent technique (*in situ* hybridization, immunocytochemistry, …) depending on the molecular phenomena that we want to study. Describing the acquisition and analysis of the fluorescent section is out of the scope of this paper. What follows, therefore, describes only the protocol used for the H&E stained sections. Low magnification (2.5X) images of all the sections are automatically acquired using a motorized Zeiss Axioplan I microscope coupled with a monochrome XilliX Microimager CCD camera. This is done by automatically scanning the area of the slide occupied by tissue, and tiling together all the individual snapshots into a single whole-view image of the sections. The sequence of microscope movements and camera operations is determined by an application running on the UNIX Ultra 10 workstation that drives both the camera and all moving parts of the microscope.

The next step consists of annotating the structures of interest (ducts, lymph nodes, tumors, …) in the images of the H&E stained sections. These annotated structures are then used to render a three-dimensional model of the tissue block where the morphology of the sample helps in determining which are the areas of the tissue where a molecular analysis may be more interesting. After selecting these areas in the three-dimensional rendition of the organ, the system asks the user to place the right fluorescent section(-s) on the stage, and high magnification (40-100X) images of the chosen areas are acquired. Finally, quantification routines are run on these new images and results are collected.

Manually annotating tissue structure in complex sections, in tissue blocks containing at least tens of sections, is feasible but for all purposes impractical due to the tremendous human effort involved. Although it might be the most accurate and reliable approach, it is not possible to carry out except when reconstructing small, simple tissue volumes. In consequence, we have developed automatic methods that eliminate or greatly reduce human interaction, thus making the reconstruction of complex systems possible. What follows describes our approach.

2.2 Image Processing
2.2.1 Preprocessing

The algorithm that we use to acquire images of entire sections creates a mosaic from a set of snapshots, each of which is the image of a single field of view. This approach causes the formation of a background pattern throughout the image (figure 2a), involving relatively large brightness gradients in between elements of the final mosaic. Now, there is no reason why an object of interest could not expand over several fields of view. Since our segmentation approach depends largely on the brightness gradients of the image, we need to eliminate the background pattern in order to obtain good segmentation results.

We achieve this goal by executing a set of arithmetic operations on the "mosaic" image. First we need a "phantom" image, that is, an image of an empty field of view taken under the same illumination conditions and microscope configuration that we used to acquire the initial image. Since all the images that we acquire have an empty frame in the upper left corner, we chose that frame as our "phantom" for the corresponding section. We then compute the average brightness of that "phantom" frame and add it to each pixel of the initial mosaic. We invert each frame of the mosaic and subtract from each one of them the inverse of the phantom image. The resulting mosaic is an inverted, background-corrected image. By doing a final inversion we get the image we were looking for (figure 2b).

2.2.2 Preliminary segmentation: Fast marching method

To obtain a first approximation of the structures that need to be segmented we use the fast marching method. We will now review the basics of this method. Consider a monotonically advancing front with speed F always positive (it could also be always negative) in the normal direction. Let $T(x, y)$ be the time at which the curve crosses the point (x, y). It is obvious that the gradient of the arrival time is inversely proportional to the speed of the function, that is,

$$|\nabla T|F = 1. \quad (1)$$

This is a form the Eikonal equation, which is very closely connected with the notion of viscosity solutions. These solutions can be achieved either by iteration or by stationary construction of $T(x, y)$. The algorithm that we use relies on the later approach. If we assume that our domain is the unit box, and imagine that the initial front is along the line $y = 0$, we can see that the front propagates upward off the initial line. Using the right approximation to the gradient, we are looking for a solution in the domain to:

$$\left[\max\left(D_{i,j}^{-x}T,0\right)^2 + \min\left(D_{i,j}^{+x}T,0\right)^2 + \max\left(D_{i,j}^{-y}T,0\right)^2 + \min\left(D_{i,j}^{+y}T,0\right)^2\right]^{\frac{1}{2}} = \frac{1}{F_{i,j}}, \quad (2)$$

where D^- and D^+ are backward and forward difference operators. This is in essence a quadratic equation for the value at each grid point, and thus we can solve the equation at each of these points and take the largest possible value as the solution. Hence, the algorithm rests on building a solution outwards from the smallest T value. The building zone is confined to a narrow band around the front.

First we need to initialize three lists: *Visited* contains the points (i, j) at which the value for T is already fixed (initially just the seed points with $T = 0$); *Close* contains the set of all grid points in the narrow band, whose T value we set as inversely proportional to $F_{i, j}$; and *Far* contains the rest of the grid points ($T = \infty$). After this we start marching forward. We remove the point in *Close* with smallest T value and we add it to *Visited*. Then we move all (if any) of the 4 connected neighbors of this point that are in *Far* to *Close*, and finally recomputed the T value for all the points in *Close* before we iterate (look for the point in *Close* with the smallest T value, …). Figure 3 shows a snapshot of a 2D grid after some iterations of this algorithm.

It is evident that an efficient version of this algorithm relies on being able to find the point with smallest value for T in the narrow band as fast as possible. Using a *min*-heap data structure to store the values of T for the points in the narrow band together with the indices that give the location of those points on the grid we achieve that goal. The *min*-heap is a complete binary tree where the value at any given node is less than or equal to the values at its children. Therefore, the point with smallest T value is always located at the root of the tree.

Finally, we define the speed of propagation in the normal direction as a decreasing function of the brightness gradient $|\nabla I(\mathbf{x})|$, that is, a function that is very small near big image gradients (i.e. possible edges) and vice versa:

$$F(x) = e^{-a|\nabla I(\mathbf{x})|}, a > 0, \quad (3)$$

where α is the "edge strength", or importance that we give to the presence of a brightness gradient in order to slow down the front. Depending on this value the speed function falls to zero more or less rapidly, and thus, it could stop few grid points away from the real edge. Also, variations in the gradient along the boundary can cause inaccurate results. False gradients due to noise can be avoided using an edge preserving smoothing scheme on the image as a preprocessing step.

The user can run the fast marching flow from a given set of initial seeds (mouse clicks on the background of the images). Alternatively, the user can decide to segment only the structures within a manually defined rectangular region of interest. If the region is too big, subsampling can be used so that the segmentation process is not to slow. This option must be used carefully, since subsampling distorts the definition or completely obliterates small structures. The resulting contour

(or contours in the case that we are segmenting several objects at the same time) will provide an excellent initial condition for the level set method.

Putting al these elements together we can get a good approximation of the shape of the object that we are trying to segment (figure 4). In order to improve the final segmentation we propose to run a few iterations of the level set method using the result of the fast marching method as the initial condition.

2.2.3 Final segmentation: Level set method

Once we have obtained a good approximation of the shape of the object using the fast marching method, we can afford to use the more computationally expensive level set method to improve the result of the segmentation. The essential idea here is to embed our marching front as the zero level set of a higher dimensional function $y(x, y, z) = \pm d$, where d is the signed distance from (x, y) to the front (figure 5). Using the chain rule we can find the motion equation:

$$y_t + F(x, y, z)|\nabla y| = 0, \quad (4)$$

where F is again the speed in the normal direction and the subscript denotes a partial derivative with respect to time. This is an initial value partial differential equation, since it describes the evolution of the solution on the basis of an initial state. As pointed out before, the level set approach offers several advantages: the zero level set of the function can change topology and form sharp corners; a discrete grid can be used together with finite differences to approximate the solution; intrinsic geometric quantities like normal and curvature can be easily extracted from the higher dimensional function; and everything extends directly to three dimensions.

If we now let the surface move with a speed $F = 1 - eK$, where $K(\mathbf{x})$ is the curvature and $e > 0$, we have a two component speed function. The constant term of F causes the front to seek object boundaries, and the curvature component controls the regularity of the deforming shape: it forces relaxation of the contour and smoothing of sharp corners. The bigger we make e, the more importance we give to this "motion by curvature" term.

To mold the initial contour (in our case the result of the fast marching method) into the desired shape we use two force terms. One of them is very similar to the one shown in equation 3, and the other one attracts the front towards the object boundaries, providing an stabilizing effect when the brightness gradient has large variations. By substituting these two terms in the motion equation we get:

$$y_t + g_I(1 - eK)|\nabla y| - b\nabla P \cdot \nabla y = 0, \quad (5)$$

where,

$$g_I(\mathbf{x}) = \frac{1}{1 + |\nabla I(\mathbf{x})|}, \quad P(\mathbf{x}) = -|\nabla I(\mathbf{x})|. \quad (6)$$

As before, $I(\mathbf{x})$ is the image, optionally smoothed using an edge-preserving smoothing scheme. P is a potential field that attracts the front towards edges in the image. This attraction is controlled by a parameter, b. $\nabla P \cdot \nabla y$ is the projection of an attractive force vector on the surface normal.

We can use the result of the fast marching method, $T(x, y)$, as the initial condition for the level set algorithm: $y(x, y; t = 0) = T(x, y)$. By solving equation 5 for a few time steps using the narrow band approach as well, we obtain an accurate segmentation of the desired object (figure 6).

3. RESULTS

In this section we consider the problem of reconstructing some intraductal cancer areas in a tissue biopsy of a cancerous human breast and a set of ducts in an entire mouse mammary gland. The tissue samples were sliced, and we used 56 sections for the human case and 70 for the mouse one. Therefore, manually segmenting each of the structures in every section is an extremely expensive process. To automatically segment them using the fast marching-level set method previously described, we begin by defining a ROI where we will run the segmentation. This ROI can be extended to cover the entire section, but then, considering the size of the images, it is wise to use subsampling in order to run the algorithm in real time.

Then we are presented with a panel (figure 7) where we can select the parameters of the algorithm. We have observed that a particular set of parameters is frequently good enough to segment similar structures (i.e., all the tumors, or all the ducts, or all the lymph nodes, …) throughout all the sections of a particular tissue block. The set of parameters that can be customized are:

- *Delta t*: how often we update the level set function inside the narrow band.
- *Move fronts outwards/inwards*: direction of expansion of the fronts, i.e., sign of the speed function. Inwards expansion is used when the initial seed is a polygon drawn around the structure of interest. Otherwise, outwards is used most of the time.
- *Epsilon*: weight of the "motion by curvature" term in the motion equation of the level set algorithm. The bigger this value, the more relaxation we force on the expanding front, and the smoother the result.
- *Beta*: weight of the attraction that edges exert on the fronts in the level set motion equation.
- *Narrow-band width*: normalized width of the narrow band used in both the fast marching method and the level set algorithm. Higher values render more accurate results, at the expense of increased computations.
- *FMM time*: how long the fast marching method will run.
- *Number of iterations of LS method*: how many iterations of the level set method to run. Normally, the number of steps positively correlates with the accuracy of the final segmentation. However, an excess in the number of steps, besides dramatically increasing computing time, can produce oversegmentation if the convergence of the algorithm is not guaranteed due to incomplete contours or image artifacts
- *Min. contour length*: size filter: size (in pixels) of the smallest segmented object that will not be discarded as noise.
- *Max. contour length*: size filter. This is the maximum size allowed for a segmented object.
- *Use FMM*: determines if the fast marching method should be used to obtain a preliminary result or not. At times, for small features, it is possible to just use the level set method from the initial seed.
- *Subsample*: determines whether the ROI must be subsampled.
- *Subsampling level*: amount of subsampling. More should be used with increasing image sizes, without compromising the resolution and level of detail of the final segmentation. An option would be to use an "imperfect" result, calculated from the subsampled image as the initial condition for a few steps of the level set method on the full resolution image.
- *Preprocessing*: The user can select to de-noise the original image using Gaussian smoothing.

After selecting the parameters of the flow, seed points are defined inside (to find the internal contour) or outside (to find the external contour) of the structures of interest. In most cases one click is enough. Large images may require several, evenly distributed clicks. The value of $T(\mathbf{x})$ at these points is set to zero, and the initial heap is constructed from their neighbors in order to start running the fast marching method. When this method finishes, the final $T(\mathbf{x})$ function is passed as the initial condition to the level set motion equation (eq. 5). We solve that equation for a few steps. This segmentation scheme provides a result in less than one second for images whose size (after subsampling, if any) is around 2 kilobytes (e.g., 512 x 512 pixels) running on a Sun Ultra 10 workstation with 1 GB of RAM.

Figures 8 and 9 show two examples of the results obtained with the combination of the fast marching and the level set methods. Figure 8b shows the segmentation of a tumor mass in a human tissue block. The results of the segmentation can be edited and removed with the interactive tools provided by our system (figure 8c). An area was selected around the

structures of interest in the section. No subsampling was used. The initial seeds are represented by blue points in figure 8a. In figure 9 we can see the segmentation of the external contours of three ducts in a particular area of an entire mouse mammary gland. In this case we also run the algorithm on a ROI on one of the sections with no subsampling factor. Figure 9a shows the points that were used as initial seeds. Figures 9b and 9c show the results of the segmentation before and after interactive correction.

Finally the segmented shapes are connected (manually) between sections, and three-dimensional reconstructions of the samples are built. Figure 10 shows a reconstruction of the tumors contained in the human tissue block that contains the tumor shown in figure 8. Surface noise can be reduced by increasing the "motion by curvature" term, as described in the methods section. In figure 11 we can see the reconstruction of the normal ducts segmented in the images of the mouse mammary gland (see figure 9).

4. DISCUSSION

Three-dimensional reconstruction of thick tissue-blocks from serial sections is an important aid for morphological analysis of normal and diseased mammary gland specimens. In this paper we have presented a method that reduces the time and interaction needed to build the three-dimensional model of a tissue block, enormously increasing the throughput of the analysis and by doing so making it feasible to use this approach for the analysis of complex, large specimens. To achieve this goal we have combined image processing techniques and two well-established schemes for interface propagation: the fast marching method and the level set method.

Our approach starts by correcting the background of the images. This is an important step, since the background pattern generated when an image is acquired modifies the brightness gradient of the image, and the speed functions that we use for interface propagation depend on that gradient. Once the background has been corrected, we run the fast marching method. This technique provides a good approximation of the boundaries of the objects that we are trying to segment in a very short time, since it assumes monotonic speed functions (always positive or always negative). We then use the approximation provided by the fast marching method as the initial condition for the level set method. This more computationally expensive algorithm is run just for a few steps, which are enough to fit the front to the contours of the structures of interest, but not as many as to make the segmentation too expensive. Finally, the option to subsample large images can enormously reduce the time required for the segmentation.

This approach can still be improved. We are currently working on a time-step independent scheme that is expected to be faster than the current one. To improve the accuracy of the results, we have developed an edge-preserving smoothing algorithm based on Beltrami's flow[11], which will replace the Gaussian smoothing currently used before executing the segmentation methods. This algorithm eliminates false gradients due to noise while enhancing gradients due to object boundaries, thus allowing the front to fit the boundaries of the object more accurately. Finally, the level set approach is readily extensible to 3D. Being able to segment three-dimensional structures of interest versus two-dimensional ones would save the process of connecting the segmented 2D contours from section to section, thus improving the analysis time. Also, since geometric properties can be easily extracted from the higher dimensional function, we could easily obtain some information about the extracted volume from the segmentation algorithm itself.

REFERENCES

1. Fernandez-Gonzalez R., Jones A., Garcia-Rodriguez E., Chen P.Y., Idica A., Barcellos-Hoff M.H., Ortiz de Solorzano C. "A system for combined three-dimensional morphological and molecular analysis of thick tissue samples", *Microscopy Research and Technique*, Vol. 59(6), pp. 522-530, December 2002.

2. Moffat D. F., Going J. J. "Three dimensional anatomy of complete duct systems in human breast: pathological and developmental implications", *Journal of Clinical Pathology*, 49, pp. 48-52, 1996.

3. Ohtake T., Kimijima I., Fukushima T., Yasuda M., Sekikawa K., Takenoshita S., Abe R., "Computer-assisted complete three-dimensional reconstruction of the mammary gland ductal/lobular systems", *Cancer*, Vol. 91(12), June 15, 2001.

4. Manconi F., Markham R., Cox G., Kable E., Fraser I. S. "Computer-generated, three-dimensional reconstruction of histological parallel serial sections displaying microvascular and glandular structures in human endometrium", *Micron*, 32, pp. 449-453, 2001.

5. Kass M., Witkin A., Terzopoulos D. "Snakes: Active contour models". *International Journal of Computer Vision*, Vol. 1, pp. 321-331, 1988.

6. Malladi R., Sethian J. A., Vemuri B. C. "Shape modeling with front propagation: a level set approach". *IEEE Transactions on Pattern Analysis and Machine Intelligence*, Vol. 17(2), pp. 158-175, Feb. 1995.

7. Osher S., Sethian J. A. "Fronts propagating with curvature dependent speed: algorithms based on Hamilton-Jacobi formulation". *Journal of Computational Physics*, Vol. 79, pp. 12-49, 1988.

8. Sethian J. A. "Level Set Methods: An Act of Violence", *American Scientist*, Vol. 85 (3), May-June 1997.

9. Sethian J. A., "A marching level set method for monotonically advancing fronts", *Proceedings of the National Academy of Sciences*, Vol. 93(4), 1996.

10. Malladi R., Sethian J. A. "A real time algorithm for medical shape recovery", *Proceedings of International Conference on Computer Vision,* pp. 304-310, Mumbai, India, January 1998.

11. Kimmel R., Malladi R., Sochen N. "Image Processing via the Beltrami Operator", *Proceedings of Asian Conference on Computer Vision,* Vol. 1351, pp. 574-581, Hong Kong, January 1998.
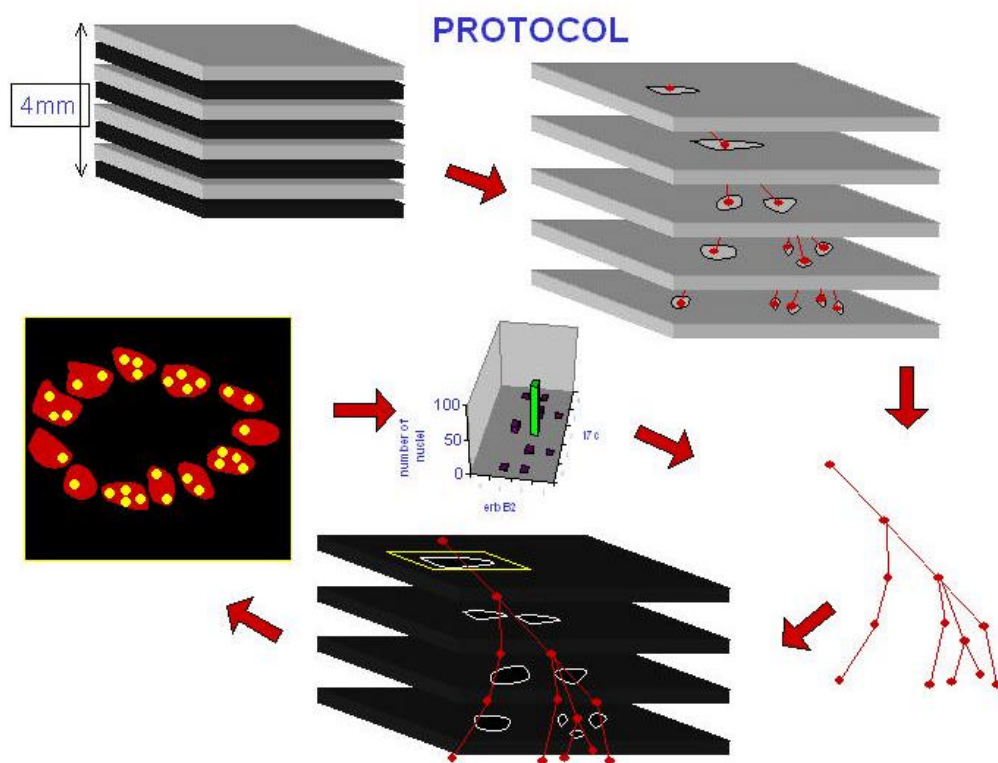
Figure 1: Protocol followed on tissue blocks. The different steps (sectioning, annotation, reconstruction, high magnification acquisition and molecular analysis) are illustrated.
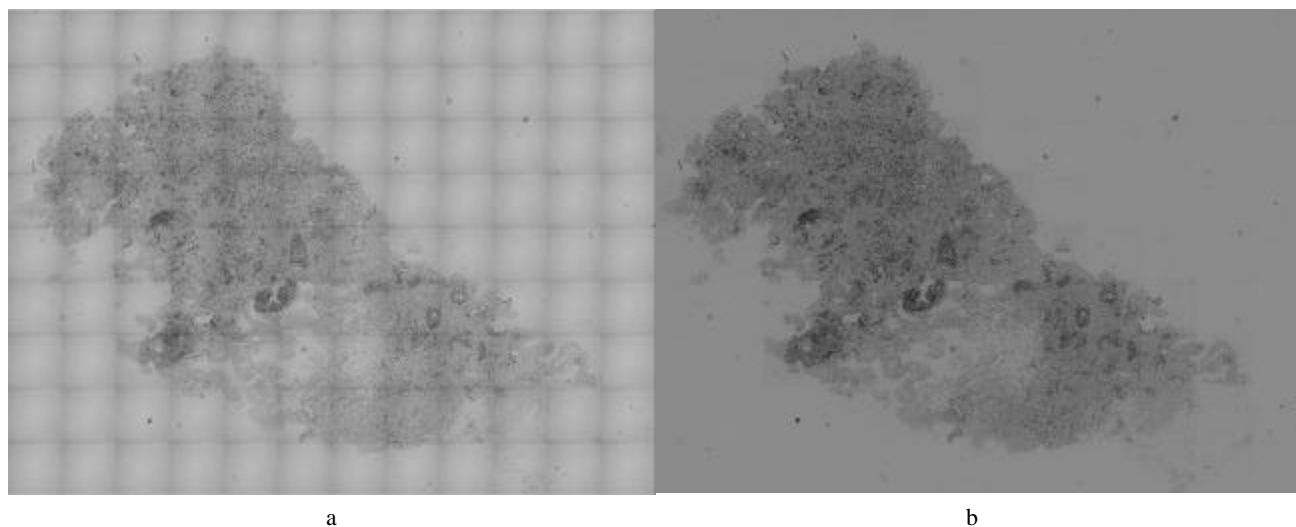

Figure 2: Background correction. a) Image of a section belonging to the human case. The background pattern created by the acquisition method is evident. b) Same image after background correction.
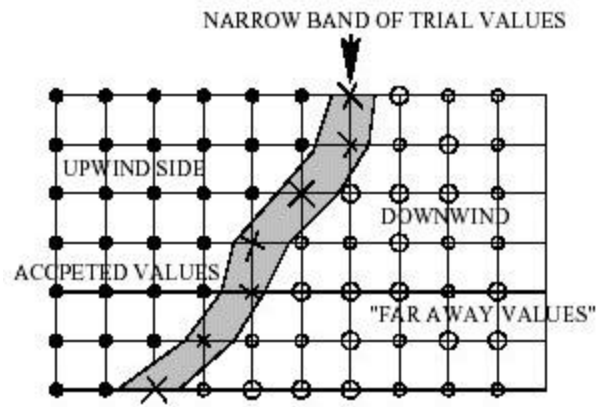
Figure 3: Snapshot of a 2D grid after several steps of the fast marching method. Accepted (*Visited*), narrow-band (*Close*) and far away (*Far*) elements are displayed.
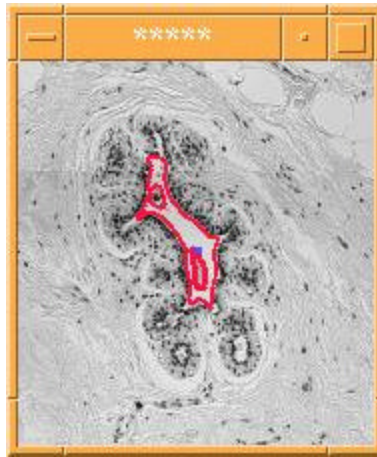
Figure 4: Result of the fast marching method on a duct in a human mammary gland tissue block. The dark point in the middle of the duct is the initial seed.
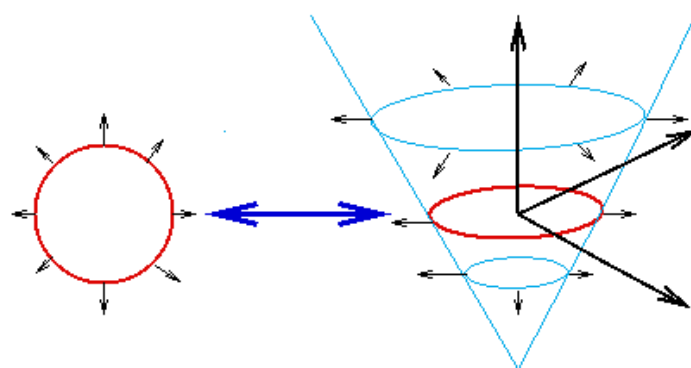
Figure 5: Basic idea of the level set method. The marching front is embedded as the zero level set of a higher dimensional function.
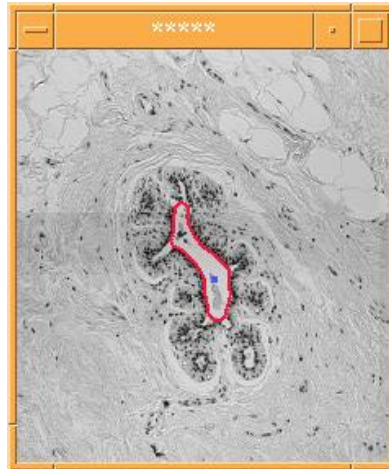
Figure 6: Result of combining the fast marching and the level set methods on the same duct that we used in figure 4. The dark point in the middle of the duct is the initial seed.

Figure 7: Options dialog. These are the parameters that the user can modify: *Delta T*, direction of front expansion, *Epsilon*, *Beta*, *Narrow band width*, *FMM time*, *Number of iterations of LS method*, *Min. contour length*, *Max. contour length*, *Use FMM*, *Subsample*, *Subsampling level* and *Preprocessing*.
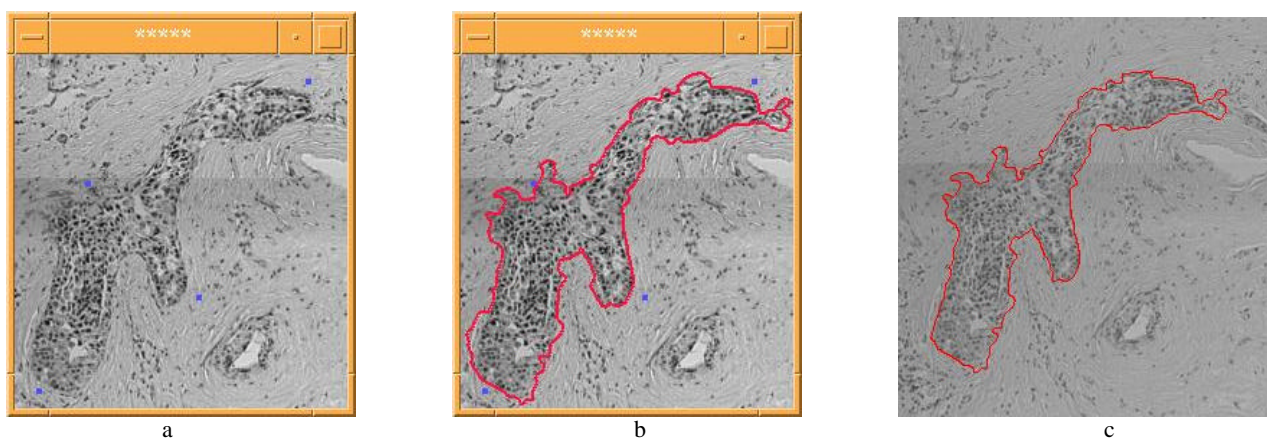
Figure 8: Segmentation of a tumor in human mammary gland tissue. a) Initial "seed" points (blue dots). b) Results of the segmentation. Red lines delineate tumor masses. c) Results after adding the result to the original image and editing using the interactive tools provided by the system.
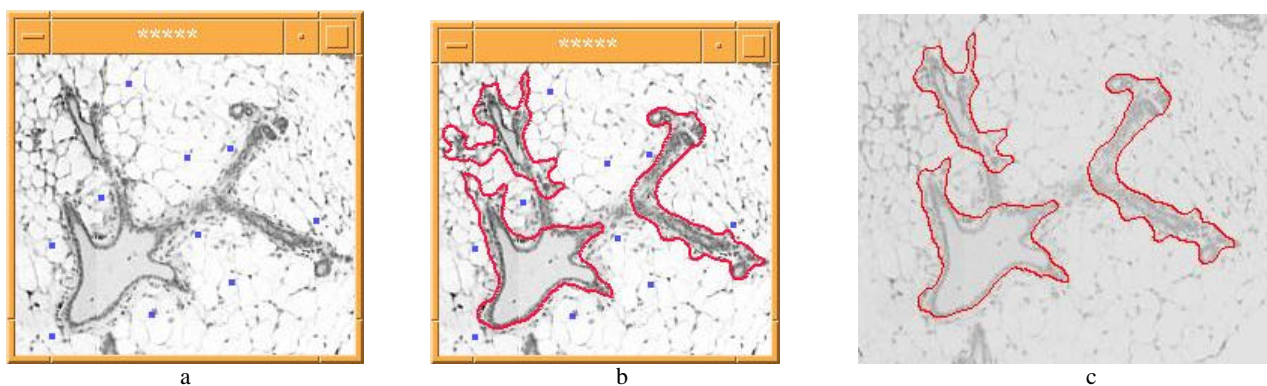

Figure 9: Segmentation of normal ducts in mouse mammary gland tissue. a) Initial "seed" points (blue dots). b) Results of the segmentation. Red lines delineate normal ducts. c) Results after adding the result to the original image and editing using the interactive tools provided by the system.
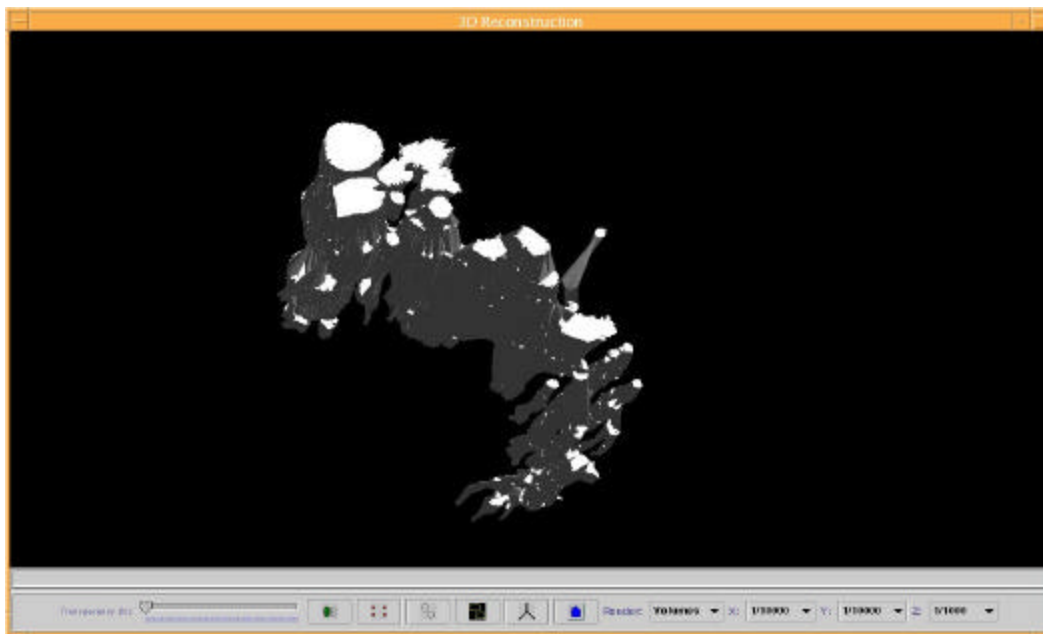
Figure 10: 3D reconstruction of tumors in a human mammary gland tissue block. Tumor masses are rendered as gray volumes. Notice the difference in smoothness between the first few sections in the central volume and the rest of the tumor due to automatic versus manual segmentation of the contours.
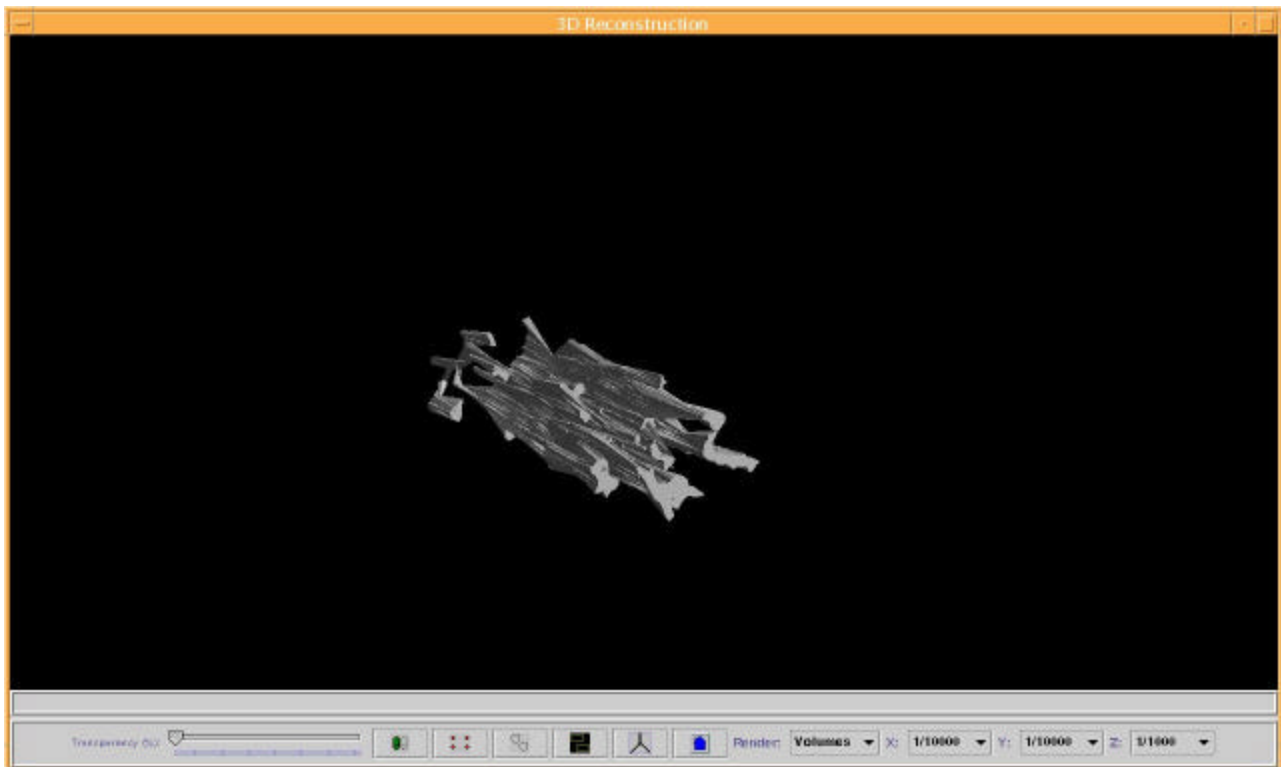

Figure 11: 3D reconstruction of normal ducts in a mouse mammary gland. Ducts are rendered as gray volumes. A single duct and its branches can be traced throughout the gland.